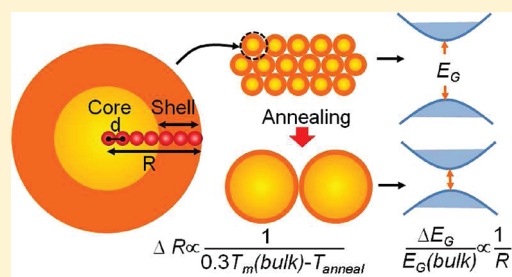


Controlling the Band Gap of ZnO by Programmable Annealing

Shouzhi Ma,[†] Houkun Liang,[‡] Xiaohui Wang,[§] Ji Zhou,[§] Longtu Li,[§] and Chang Q Sun^{*,†}[†]School of Electric and Electronic Engineering, Nanyang Technological University, Singapore 639798[‡]Singapore Institute of Manufacturing Technology, 71 Nanyang Drive, Singapore 638075[§]State Key Laboratory of New Ceramics and Fine Processing, Department of Materials Science and Engineering, Tsinghua University, Beijing 100084, China

ABSTRACT: Annealing has been extensively used to control crystal growth and physical properties of materials with unfortunately unclear mechanism and quantitative correlations. Here we present the “annealing temperature—grain size—band gap” correlation for ZnO nanocrystals with experimental evidence. Findings revealed that the annealing condition determines the critical size by equating the thermal and the cohesive energy of the undercoordinated atoms in the surface skin, which in turn induce local strain and quantum entrapment, perturbing the Hamiltonian and hence the band gap. The formulation provides a general guideline for controlling crystal growth and performance of materials and makes predictive design and fabrication of functional nanomaterials a reality.



I. INTRODUCTION

With the miniaturization of crystal size, the fraction of undercoordinated surface atoms becomes dominant, and hence, materials in the nanoregime behave differently from their bulk counterpart. Many features of the material are no longer constant but become tunable with size. For example, the band gap (E_G) of ZnO nanostructures becomes tunable,¹ which is of profound importance to the optical device design such as light emitters² and laser diodes.³ One effective means being widely used to tune the grain size and the E_G of nanoparticles (NPs) is thermal annealing. Experimentally, the narrowing of the E_G resulting from annealing ZnO NPs has been observed by Zak et al.⁴ By comparing the photoabsorption (PA) and photoluminescence (PL) spectra, Lin et al.⁵ observed an increase in the Stoke shift as the particle size decreased. However, one challenging issue is that the annealing process is usually based on a trial-and-error approach which lacks theoretical guidelines. On the other hand, the effects of particle size on the energy of photoabsorption (E_{PA}),⁶ photoluminescence (E_{PL}),⁷ and their correlation remain unclear despite models such as quantum confinement,⁸ thermodynamics,⁹ luminescence center,¹⁰ free-exciton collision,¹¹ and surface states.¹² These models explain phenomenologically well the energy shift of either the E_{PA} or the E_{PL} alone. However, the relationship among annealing temperature, grain size, E_{PA} , and E_{PL} remains a challenge. A quantitative correlation between the annealing temperature and the derived physical properties pursued is therefore highly desired. In fact, the annealing temperature, the crystal size, and the band gap are interconnected. In this work, we propose and verify these size-related properties from the perspective of the bond order—length—strength (BOLS) correlation mechanism¹³ with ZnO nanocrystals as the prototype of demonstration.

II. THEORY

According to the BOLS theory,¹³ the size tenability at nano-scale arises from the tunable fraction of the undercoordinated atoms and the interaction between them.¹⁴ Recent progress showed that not only the bond length but also the bond energy changes at the surface skin of NPs in comparison with the bulk.¹⁵ The shorter and stronger bonds between the undercoordinated atoms¹⁶ provide perturbation to the Hamiltonian of the entire system especially when the system is miniaturized. As a result, the physically detectable quantities undergo a modification $Q(R_{NP}) = Q(\infty)(1 + \Delta)$, where Q denotes the physical quantity such as band gap or melting temperature, and ∞ and R_{NP} represent the bulk and finite sized NPs or grains with radius R_{NP} , respectively. Δ is the size-induced perturbation to Q . If a nanoparticle has a core-shell structure,¹⁷ Δ solely arises from the surface atoms. The effect of undercoordinated surface atoms can be modeled by BOLS correlation: denote d and E as the bond length and binding energy, respectively, and d_b , d_i , E_b , and E_i are the bond length in the bulk and in the i th atomic layer (counting from outermost inward) and binding energy in the bulk and in the i th atomic layer, respectively. For an undercoordinated atom in the i th surface layer, bonds contract from the ideal bulk value of d_b to $d_i = c_i d_b$, and the binding energy per bond increases from E_b to $E_i = c_i^{-m} E_b$, $c_i = 2 / \{1 + \exp[(12 - z_i) / (8z_i)]\}$ is the bond contraction coefficient, with z being the coordination number (CN) of a specific atom, and $m = 4$ is the bond nature indicator for ZnO.¹⁸ The shell consists of up to three atomic layers (i.e., $i \leq 3$), which suffers from bond order deficiency and hence bond length

Received: July 29, 2011

Revised: September 15, 2011

Published: September 15, 2011

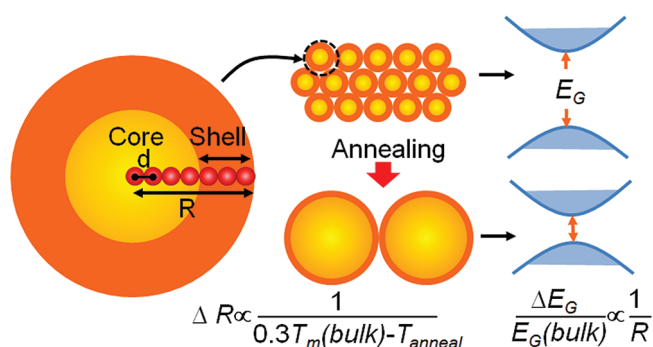


Figure 1. Schematic of the core–shell structure of a single grain and grain growth and band gap evolution resulting from thermal annealing.

contraction and bond energy gain, originating the property change. Figure 1 shows the core–shell structure of a grain. When the solid size is increased, the surface to volume ratio is significantly reduced. By employing the BOLS-induced perturbation, the unusual mechanical, thermal, electrical, optical, and acoustic behaviors resulting from vacancies and adatoms, defects, nanostructures, and size effect can be unified.

According to the nearly free electron approximation, E_G depends uniquely on the first Fourier coefficient of the crystal potential and is proportional to the binding energy per bond: $E_G = 2|V_1| \propto \langle E_b \rangle$. On the basis of the BOLS correlation, the perturbation to E_G is derived as

$$\begin{cases} E_G(R) = E_G(\infty)(1 + \Delta_H) \\ \Delta_H = R^{-1} \sum_{i \leq 3} \tau c_i (c_i^{-m} - 1) = R^{-1} \Delta'_H \end{cases} \quad (1)$$

where $R = R_{NP}/d$ is the normalized radius of a nanoparticle or grain, meaning the number of atoms lined along the radius (as illustrated by Figure 1). Δ_H is the Hamiltonian perturbation, and $\tau c_i R^{-1}$ is the surface-to-volume ratio, which means the proportion of atoms in the i th atomic layer to the total number of atoms in a NP as derived in ref 18. τ is the dimensionality, which equals 2 for nanowire and 3 for NPs.

Besides the band gap, the grain radius R is also tuned by annealing as presented by Figure 1. The cohesive energy, E_{coh} , determines the NP size allowed at certain temperature as the NP size is directly related to the cohesive energy.¹⁹ We have demonstrated that the size of a particle in nucleation depends on the ratio between the annealing (T_a) and the melting temperature (T_m) of the specimen, T_a/T_m .²⁰ When $T_a \approx 0.3T_m$, the particle growth is in equilibrium, and the size is stable.²¹ Larger grains require higher T_a ,²² but as a competing factor, the T_m increases with grain size.²³ It is essential to find the size effect on the T_m before quantifying the R to be tuned by T_a . T_m is proportional to the atomic cohesive energy and equals the product of bond energy and the atomic CN, i.e., $E_{coh} = zE_b$, which results in the cohesive energy perturbation Δ_{coh} containing z

$$\begin{cases} T_m(R) = T_m(\infty)(1 + \Delta_{coh}) \\ \Delta_{coh} = R^{-1} \sum_{i \leq 3} \tau c_i (z_i/z_b \times c_i^{-m} - 1) = R^{-1} \Delta'_{coh} \end{cases} \quad (2)$$

For the postannealing process, the as-grown particle size (R_0) and threshold temperature (T_{th}) need to be involved. The high-energy grain boundary does not gain mobility until reaching

Table 1. Grain Radius Derived from XRD fwhm and SEM Micrographs for ZnO Annealed at Different Temperatures and Experimentally Measured E_{PA} and E_{PL}

temperature (K)	fwhm	XRD (nm)	SEM (nm)	E_{PA} (eV)	E_{PL} (eV)
573	0.4	10	10	3.339	3.234
673	0.37	11	11	3.330	3.213
773	0.29	14.5	15	3.315	3.202
823	0.25	16.5	17.5	3.282	3.142
873	0.22	18.5	18.5	3.264	3.123
923	0.21	20	25	3.249	3.108
973	0.16	25	40	3.220	3.099

T_{th} ,²⁴ at which grains grow upon heating to minimize the overall energy. With T_{th} and R_0 in consideration, eq 3 gives the completed expression for critical size R allowed by the respective T_a

$$\begin{cases} T_a - T_{th} = 0.3T_m(R) = 0.3T_m(\infty)(1 + R^{-1}\Delta'_{coh}) \\ R - R_0 = \frac{\Delta'_{coh}}{(T_a - T_{th})/[0.3T_m(\infty)] - 1} = \frac{|\Delta'_{coh}|}{1 - (T_a - T_{th})/[0.3T_m(\infty)]} \end{cases} \quad (3)$$

This relation indicates that the crystal size is dominated by the term $(T_a - T_{th})/[0.3T_m(\infty)]$; the grain grows as T_a rises when $T_a > T_{th}$. For a given T_a , the grain radius R is hence predictable.

III. EXPERIMENTS

To verify the theoretical predictions of grain size and band gap tuned by the annealing process, polycrystalline ZnO thin film of 10 nm grain radius was deposited on a quartz substrate using an arc deposition technique.²⁵ A postannealing process at 573–973 K in air for 1 h tuned the grain radius to 10–40 nm. The grain sizes were measured using X-ray diffraction (XRD) and scanning electron microscopy (SEM). XRD measurements revealed that the samples were polycrystalline with a hexagonal wurtzite structure and had a preferred (002) orientation. In the ZnO films, the amount of impurities and defects is neglectably small. The grain size was determined from the full width at half-maximum (fwhm) of the (002) peak (i.e., $2\theta = 34.5^\circ$) of the XRD profiles, according to Scherrer's equation with $\lambda = 0.154$ nm for Cu K_α radiation. Table 1 summarizes the grain size derived from XRD and SEM results. The SEM inspection shows agreement with the XRD measurements. To study the size effect on the optical band gap at room temperature, the PL spectrum was acquired using the Nd:YAG (355 nm) pulsed laser (10 Hz). The absorption was measured on a double-beam spectrophotometer. The measured E_{PA} and E_{PL} for different grain sizes are also summarized in Table 1.

IV. RESULTS AND DISCUSSION

The as-grown grain radius is 10 nm, so $R_0 = 10 \text{ nm}/0.199 \text{ nm}^{-1} = 50$ after normalization. There is no obvious grain growth below 573 K, indicating that 573 K is the T_{th} . According to eq 3, grain size tuned by different T_a can be theoretically predicted as shown in Figure 2. Experimental results show good agreement with expectations, especially before the grains gain fast growth. The stable grain size increases rapidly with temperature when the T_a is above 900 K. At higher T_a , although there is an increase in discrepancy between experiments and calculation, the deviation

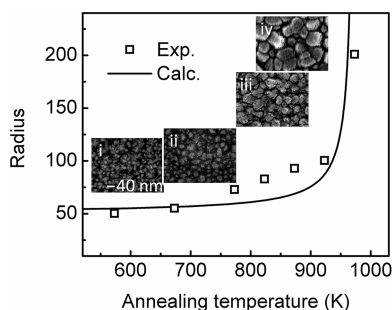


Figure 2. Comparison of theoretically predicted R (normalized) with that experimentally measured from XRD and SEM. The inset shows the SEM micrograph of ZnO NPs annealed at different temperatures: (i) as-grown grains, and grains annealed at (ii) 773 K, (iii) 873 K, and (iv) 973 K.

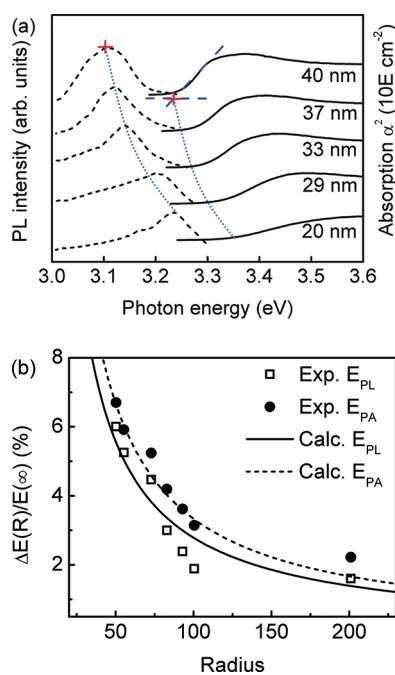


Figure 3. (a) Experimentally measured photoluminescence and absorption spectrum for various grain diameters. (b) Experimental and theoretical E_{PA} and E_{PL} blue shift for different grain radius R (normalized).

does not have a strong effect as the grains are in the submicrometer regime and surface atoms gradually lose their hegemony. The inset shows the SEM micrograph of spontaneous grain growth at different temperatures. By employing the coordination and bond length correlation, the cohesive energy is found to be proportional to the inverse grain radius. As T_a increases, the stable grain size is determined by the decreased surface to volume ratio. Consistency between experiment and calculation confirms the validity of BOLS theory, which can provide guidelines for controlling thermal annealing.

The absorption coefficient was derived from the transmission spectra according to $I = I_0 \exp(-\alpha x)$. For direct band gap materials, the absorption coefficient $\alpha \propto \sqrt{(h\nu - E_G)}$. α^2 versus photon energy $h\nu$ was derived from the transmission spectra as shown in Figure 3(a). By using the linear fitting of the absorption edges, the E_{PA} values were derived and found to be blue-shifted

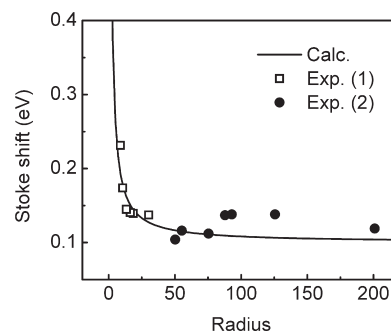


Figure 4. Experimentally measured and theoretically calculated size-dependent Stoke shift for various grain radius R (normalized). Data of Exp. (1) are from ref 5 and of Exp. (2) are from our experiment.

with the decrease of the particle size. To estimate the difference between E_{PA} and E_{PL} , the PL spectra were also shown in Figure 3(a) for comparison. In the PL spectra, near-band-edge emissions were observed in all of the films. The peak positions were also blue-shifted with the decrease of the particle size. The shift arises from the size effect as illustrated by eq 1. Comparing the PA and PL spectra, one can note that the E_{PL} is lower than the E_{PA} . The energy offset, i.e., Stoke shift (E_{SS}), as theoretically²⁶ explained and experimentally²⁷ verified, is due to the lattice vibration and exciton binding energy. In our experiment, E_{SS} is around 0.1 eV, which agrees with documented values²⁸ except that Lin et al.⁵ have observed a much larger E_{SS} . Since E_{SS} comes from electron–phonon coupling and crystal binding²⁹ in a crystal lattice, it is size dependent: for a single bond, $E_{SS} \propto q^2$ with q being in the dimension of the wave vector. q is inversely proportional to atomic distance d , and hence, $E_{SS} \propto A/d^2$ in the surface region where A is a constant depending on the band curvature. It has already been shown that the bonds shrink in the surface layers. On the basis of the BOLS premise, E_{SS} can be correlated to the bond contraction and expressed as

$$E_{SS} = AR^{-1} \sum_{i \leq 3} \tau c_i (c_i^{-2} - 1) E_{PL} + 0.1. \quad (4)$$

Equation 4 indicates that E_{SS} consists of two terms: the first term represents the size-originated energy shift due to bond contraction, and the second term is the empirical bulk E_{SS} which is around 0.1 eV.²⁸ To estimate the size effect on E_{PL} and E_{PA} , both the Hamiltonian perturbation and the Stoke shift should be involved. Figure 3(b) shows the comparison of the experimentally observed and theoretically predicted energy shift ΔE in the PA and PL spectrum of finite-sized NPs with respect to their corresponding bulk energy $E(\infty)$ versus normalized grain radius. The calculated E_{PA} and E_{PL} are $E_{PA} = E_G + 1/2E_{SS}$ and $E_{PL} = E_G - 1/2E_{SS}$, where E_G and E_{SS} are given in eq 1 and eq 4, respectively. In the process of excitation and recombination, an electron absorbs a photon with energy $E_{PA} = E_{PL} + E_{SS}$ and emits a photon with energy E_{PL} . At the surface, the CN-imperfection-enhanced bond strength affects both the Stoke shift and the band gap. Good agreement between predictions and measurements proved the validity of the BOLS correlation. Our experiments suggested that E_{PA} and E_{PL} for bulk are 3.15 and 3.05 eV, respectively. Figure 4 shows the good match of the calculated E_{SS} based on eq 4 with experimental data. The large E_{SS} in Lin's experiment (i.e., $R < 40$) can be explained by size effect. The grain size is so small that the size-dependent term in eq 4 dominates; the first term in eq 4 is significant enough to increase the E_{SS} from

0.1 to 0.3 eV due to increased surface to volume ratio. The blue shift of E_{PA} and E_{PL} is the joint contribution from the crystal binding and the electron–phonon coupling. Without the bond contraction, neither E_G expansion nor PA or PL blue shift will happen; the summation over all the volumes will not be R dependent.

There are a number of experiments on optical properties of ZnO nanostructures which support our analytical model. For example, Zak et al.⁴ found that annealing increases the size for ZnO NPs, associated with a narrowing of the optical band gap. The PL and PA blue shift and Stoke shift of ZnO quantum dots measured by Lin et al.⁵ are in agreement with the BOLS correlation. The same trend of Stoke shift has also been observed for other direct band gap materials besides ZnO.³⁰ Documented experimental band gap varies with synthesis methods and measuring technique. In our experiment, the bulk absorption band gap is 3.15 eV, which is smaller than the literature.¹ Srikant and Clarke³¹ observed that the band gap of ZnO derived from absorption was lower than that from other methods such as spectroscopic ellipsometry, possibly because the transmittance measurement probes both the surface and bulk of the sample while other popular methods only probe the surface. This conclusion provides evidence for the significance of bond deficiency and bond enhancement at surfaces.

V. CONCLUSION

In conclusion, an analytical correlation between the “annealing temperature–grain size–band gap” has been established toward consistent understanding of the annealing-controlled ZnO synthesis and band gap. The findings demonstrated that the annealing-induced grain size and band gap change are attributed to the surface and interface atomic CN deficiency and bond energy perturbation. Annealing tunes the equilibrium atomic cohesive energy, while the perturbation to Hamiltonian determines the band gap. Exceedingly good agreement between predictions and measurements indicates that the broken bond in the surface layers is the essential cause for the temperature-driven grain growth and spontaneous band gap shift.

AUTHOR INFORMATION

Corresponding Author

*Phone: (65)67904517. E-mail: ecqsun@ntu.edu.sg.

ACKNOWLEDGMENT

The work was supported by the National Science Fund for distinguished young scholars (No. 50625204), Science Fund for Creative Research Groups (No. 50621201), and the Ministry of Sciences and Technology of China through National Basic Research Program of China (973 Programs under Grant No. 2009CB623301).

REFERENCES

- (1) Özgür, Ü.; Alivov, Y. I.; Liu, C.; Teke, A.; Reshchikov, M. A.; Doğan, S.; Avrutin, V.; Cho, S.-J.; Morkoc, H. *J. Appl. Phys.* **2005**, *98*, 041301.
- (2) Dai, J.; Xu, C. X.; Wu, P.; Guo, J. Y.; Li, Z. H.; Shi, Z. L. *Appl. Phys. Lett.* **2010**, *97*, 011101–011103.
- (3) Lim, J. H.; Kang, C. K.; Kim, K. K.; Park, I. K.; Hwang, D. K.; Park, S. J. *Adv. Mater.* **2006**, *18*, 2720–2724.

- (4) Zak, A. K.; Abrishami, M. E.; Majid, W. H. A.; Yousefi, R.; Hosseini, S. M. *Ceram. Int.* **2011**, *37*, 393–398.
- (5) Lin, K.-F.; Cheng, H.-M.; Hsu, H.-C.; Lin, L.-J.; Hsieh, W.-F. *Chem. Phys. Lett.* **2005**, *409*, 208–211.
- (6) Nie, J. C.; Yang, J. Y.; Piao, Y.; Li, H.; Sun, Y.; Xue, Q. M.; Xiong, C. M.; Dou, R. F.; Tu, Q. Y. *Appl. Phys. Lett.* **2008**, *93*, 173104.
- (7) Chen, Y.; Tuan, N. T.; Segawa, Y.; Ko, H.-j.; Hong, S.-k.; Yao, T. *Appl. Phys. Lett.* **2001**, *78*, 1469–1471.
- (8) Cheng, H.-M.; Lin, K.-F.; Hsu, H.-C.; Hsieh, W.-F. *Appl. Phys. Lett.* **2006**, *88*, 261909.
- (9) Yang, C. C.; Li, S. J. *Phys. Chem. C* **2008**, *112*, 2851–2856.
- (10) Qin, G. G.; Song, H. Z.; Zhang, B. R.; Lin, J.; Duan, J. Q.; Yao, G. Q. *Phys. Rev. B* **1996**, *54*, 2548–2555.
- (11) Glinka, Y. D.; Lin, S.-H.; Hwang, L.-P.; Chen, Y.-T.; Tolk, N. H. *Phys. Rev. B* **2001**, *64*, 085421.
- (12) (a) Chen, C.-W.; Chen, K.-H.; Shen, C.-H.; Ganguly, A.; Chen, L.-C.; Wu, J.-J.; Wen, H.-I.; Pong, W.-F. *Appl. Phys. Lett.* **2006**, *88*, 241905. (b) Wang, X.; Qu, L.; Zhang, J.; Peng, X.; Xiao, M. *Nano Lett.* **2003**, *3*, 1103–1106.
- (13) Sun, C. Q. *Prog. Solid State Chem.* **2007**, *35*, 1–159.
- (14) Pauling, L. J. *Am. Ceram. Soc.* **1947**, *69*, 542–553.
- (15) Yu, R.; Hu, L. H.; Cheng, Z. Y.; Li, Y. D.; Ye, H. Q.; Zhu, J. *Phys. Rev. Lett.* **2010**, *105*, 226101.
- (16) Huang, W. J.; Sun, R.; Tao, J.; Menard, L. D.; Nuzzo, R. G.; Zuo, J. M. *Nat. Mater.* **2008**, *7*, 308–313.
- (17) Dai, S.; Dumn, M. L.; Park, H. S. *Nanotechnology* **2010**, *21*, 445707.
- (18) Ma, S.; Wang, X.; Zhou, J.; Li, L.; Sun, C. Q. *J. Appl. Phys.* **2010**, *107*, 064102.
- (19) Vanithakumari, S. C.; Nanda, K. K. *Phys. Lett. A* **2008**, *372*, 6930–6934.
- (20) Sun, C. Q.; Shi, Y.; Li, C. M.; Li, S.; Yeung, T. C. A. *Phys. Rev. B* **2006**, *73*, 075408–075409.
- (21) Romero-Gómez, P.; Toudert, J.; Sánchez-Valencia, J. R.; Borrás, Ana; Barranco, A.; Gonzalez-Elipe, A. R. *J. Phys. Chem. C* **2010**, *114*, 20932–20940.
- (22) Dutta, S.; Chattopadhyay, S.; Jana, D.; Banerjee, A.; Manik, S.; Pradhan, S. K.; Sutradhar, M.; Sarkar, A. *J. Appl. Phys.* **2006**, *100*, 114328–114326.
- (23) (a) Singh, V. N.; Mehta, B. R. *J. Nanosci. Nanotechnol.* **2005**, *5*, 431–435. (b) Guisbiers, G.; Pereira, S. *Nanotechnology* **2007**, *18*, 435710.
- (24) Kang, H. S.; Kang, J. S.; Kim, J. W.; Lee, S. Y. *J. Appl. Phys.* **2004**, *95*, 1246–1250.
- (25) Wang, Y. G.; Lau, S. P.; Lee, H. W.; Yu, S. F.; Tay, B. K.; Zhang, X. H.; Tse, K. Y.; Hng, H. H. *J. Appl. Phys.* **2003**, *94*, 1597–1604.
- (26) Fu, Z. D.; Cui, Y. S.; Zhang, S. Y.; Chen, J.; Yu, D. P.; Zhang, S. L.; Niu, L.; Jiang, J. Z. *Appl. Phys. Lett.* **2007**, *90*, 263113–263113.
- (27) Petersen, J.; Brimont, C.; Gallart, M.; Cregut, O.; Schmerber, G.; Gilliot, P.; Honerlage, B.; Ulhaq-Bouillet, C.; Rehspringer, J. L.; Leuvrey, C.; et al. *J. Appl. Phys.* **2008**, *104*, 113539–113535.
- (28) (a) Klingshirn, C. *Phys. Status Solidi B* **1975**, *71*, 547–556. (b) Bagnall, D. M.; Chen, Y. F.; Zhu, Z.; Yao, T.; Shen, M. Y.; Goto, T. *Appl. Phys. Lett.* **1998**, *73*, 1038–1040.
- (29) (a) Li, J. W.; Liu, X. J.; Yang, L. W.; Zhou, Z. F.; Xie, G. F.; Pan, Y.; Wang, X. H.; Zhou, J.; Li, L. T.; Pan, L.; et al. *Appl. Phys. Lett.* **2009**, *95*, 031906. (b) Pan, L. K.; Sun, C. Q. *J. Appl. Phys.* **2004**, *95*, 3819–3821.
- (30) (a) Nirmal, M.; Norris, D. J.; Kuno, M.; Bawendi, M. G.; Efros, A. L.; Rosen, M. *Phys. Rev. Lett.* **1995**, *75*, 3728–3731. (b) Fu, H.; Zunger, A. *Phys. Rev. B* **1997**, *56*, 1496–1508.
- (31) Srikant, V.; Clarke, D. R. *J. Appl. Phys.* **1998**, *83*, 5447–5451.